Eur. Phys. J. A (2018) **54**: 90
DOI 10.1140/epja/i2018-12525-3

THE EUROPEAN PHYSICAL JOURNAL A

Regular Article – Theoretical Physics

Fraunhofer and refractive scattering of heavy ions in strong laser fields

Şerban Mişicu[a] and Florin Carstoiu

Department of Theoretical Physics, National Institute for Physics and Nuclear Engineering "Horia Hulubei", Atomistilor 407, RO-077125, POB-MG6, Măgurele-Bucharest, Romania

Received: 12 December 2017 / Revised: 15 March 2018
Published online: 30 May 2018

Communicated by P. Capel

Abstract. Until recently the potential scattering of a charged particle in a laser field received attention exclusively in atomic physics. The differential cross-section of laser-assisted electron-atom collisions for n emitted or absorbed photons is provided by a simple law which casts the result as a product between the field-free value and the square of the Bessel function of order n with its argument containing the effect of the laser in a non-perturbative way. From the experimental standpoint, laser-assisted electron-atom collisions are important because they allow the observation of multiphoton effects even at moderate laser intensities. The aim of this study is to calculate the nucleus-nucleus differential cross section in the field of a strong laser with wavelengths in the optical domain such that the low-frequency approximation is fulfilled. We investigate the dependence of the n-photon differential cross-section on the intensity, photon energy and shape of the pulse for a projectile/target combination at a fixed collision energy which exhibits a superposition of Fraunhofer and refractive behavior. We also discuss the role of the laser perturbation on the near and farside decomposition in the angular distribution, an issue never discussed before in the literature. We apply a standard optical model approach to explain the experimental differential cross-section of the elastic scattering of ^{4}He on ^{58}Ni at a laboratory energy $E = 139\,\mathrm{MeV}$ and resolve the corresponding farside/nearside (F/N) decomposition in the field-free case. We give an example of reaction in which Fraunhofer diffraction and refractive rainbow hump effects are easily recognized in the elastic angular distribution. Next, we apply the Kroll-Watson theorem, in order to determine the n-photon contributions to the cross-section for continuous-wave (cw) and modulated pulses. In the elastic scattering of heavy ions in a radiation field of low intensity, the amplitude drops by orders of magnitude with respect to the unperturbed case once the exchange of photons is initiated. For intensities approaching $I = 10^{17}\,\mathrm{W/cm^2}$ multiphoton effects become important. In the case of short laser pulses we conclude that the strength of n-photon contribution increases with the pulse duration.

1 Introduction

In a manner analogous to the study of laser assisted collisions of atoms with electrons, we expect that nucleus-nucleus potential scattering in the presence of a strong electromagnetic field may unravel new classical and quantum features of the collisional dynamics at the nuclear level. Until now this topic was only scarcely discussed in the literature. Let us briefly review some of the theoretical aspects concerning the laser-assisted charge scattering. In early papers this problem was tackled by considering an electron moving under the simultaneous action of an electromagnetic potential and a scattering real potential [1]. This problem, also known under the name of radiative scattering, proved to be relevant in the practical context of plasma heating by intense electromagnetic fields [2], but also for theoretical predictions since the action of the laser at various intensities allows the experimental accessibility to some of the electron-atom scattering parameters that otherwise are not revealed. Thus, in the above mentioned paper of Kroll and Watson (K-W) a remarkable theorem was stated, namely for a linearly polarized laser, the differential cross section accompanied by the absorption of n photons is a simple product of the field-free elastic differential cross-section and the square of the Bessel function of order n which encodes in its argument the field parameters. The importance of this theorem consists in providing a sound approximation to multiphoton energy transfers when the frequency of the laser wave is low or when the scattering potential is weak.

Multiphoton processes accompanying laser-assisted electron-atom elastic collisions were observed for the first

[a] e-mail: misicu@theory.nipne.ro

time in an experiment by Weingartshofer *et al.* (see the review article [3] and references therein). In this type of experiment the atomic beam, which impinges perpendicularly to the scattering plane defined by the initial and final electron momenta, is crossed in coincidence with the laser and electron beams (three-beam experiment) and the scattered electrons are recorded. In the range of laser intensities 10^8–$10^{12}\,\mathrm{W/cm^2}$, an increase (decrease) of the final electrons' kinetic energies corresponding to the absorption (emission) of several photons was established.

The modification of nuclear reactions rates was only in a few occasions discussed in the literature. The resonant scattering of neutrons by nuclei in the field of a strong electromagnetic wave was investigated in [4] and the possibility to observe multiphoton effects discussed qualitatively. In ref. [5] the laser-assisted Coulomb excitation by proton projectiles was claimed to be enhanced for the intensity $10^{16}\,\mathrm{W/cm^2}$, a quite large value for the laser sources available at the beginning of eighties. Laser-assisted proton inelastic scattering on nuclei was recently considered for monochromatic [6] and bichromatic fields [7]. Compared to the previously mentioned study on Coulomb excitation, nuclear effects are included via an optical potential with Woods-Saxon (WS) form factors. The calculated one- and two-photons differential cross-sections are much lower than the corresponding $n = 0$ values, and they gradually decrease with the number of absorbed photons.

A theoretical approach to the general description of the quantum dynamics of two reacting nuclei was put forward by one of us (ŞM) and applied to the case of spontaneous α-emission from a heavy radioactive nucleus in order to compute the decay rate [8]. Using this framework we provide in section 2 of the paper a derivation of the laser-assisted differential cross section formula in the first-Born approximation based on the S-matrix formalism. In the third section we investigate the scattering of an α-particle beam on a ^{58}Ni target, first in the field-free case using an optical potential model analysis and next assisted by laser pulses of various shapes with intensities in the range 10^9–$10^{17}\,\mathrm{W/cm^2}$ and photon energies in the range 1.5–15 eV. In the last section we comment on the possible experimental conditions necessary to test the Kroll-Watson theory.

2 Nucleus-nucleus scattering in a strong electromagnetic field

In this paper we consider a colliding system composed of two heavy ions of charges $Z_{1,2}$ and masses $A_{1,2}$ in the field of a linearly polarized, monochromatic electromagnetic field by a vector potential

$$\boldsymbol{A}(\boldsymbol{r},t) = \boldsymbol{A}_0 \cos(\omega t - \boldsymbol{k}\cdot r) \tag{1}$$

corresponding to the angular frequency ω and wavelength $\lambda = 2\pi c/\omega$. In what follows this signal is dubbed as continuous-wave. Our study concerns lasers of wavelengths λ large compared to the size of the irradiated quantum system and intensities that are not too high. Consequently it is justified to retain the first term in the expansion in powers of $\boldsymbol{k}\cdot\boldsymbol{r}$ in eq. (1) and the vector potential can be safely taken as spatially homogeneous, *i.e.* $\boldsymbol{A}(r,t) \approx \boldsymbol{A}(t)$. Then, by choosing its amplitude as

$$\boldsymbol{A}_0 = \hat{\boldsymbol{\epsilon}}\frac{\mathcal{E}_0}{\omega}\,, \tag{2}$$

where $\hat{\boldsymbol{\epsilon}}$ is the polarization of the electromagnetic wave, the electric field in the dipole approximation reads

$$\boldsymbol{E}(t) = -\frac{\partial \boldsymbol{A}}{\partial t} = \hat{\boldsymbol{\epsilon}}\mathcal{E}_0 \sin\omega t. \tag{3}$$

We showed in a previous paper [8] that within this approximation, the wave-function of the nucleus-nucleus relative motion satisfies the time-dependent Schrödinger equation (TDSE),

$$i\hbar\frac{\partial\psi(\boldsymbol{r},t)}{\partial t} = \left[H_0 + H_{\mathrm{int}}(t)\right]\psi(\boldsymbol{r},t), \tag{4}$$

where

$$H_0 = \frac{\boldsymbol{p}^2}{2\mu} + V(\boldsymbol{r}) \tag{5}$$

is the time-independent Hamiltonian of the two heavy-ions, of reduced mass $\mu = mA_1A_2/(A_1+A_2)$, interacting via a static potential $V(\boldsymbol{r})$ in the absence of the laser field (field-free Hamiltonian), whereas

$$H_{\mathrm{int}}(t) = -\frac{e}{m}\left(\frac{Z_1}{A_1} - \frac{Z_2}{A_2}\right)\boldsymbol{p}\cdot\boldsymbol{A} + \frac{e^2}{2m}\left(\frac{Z_1^2}{A_1} + \frac{Z_2^2}{A_2}\right)\boldsymbol{A}^2 \tag{6}$$

is the time-dependent part of the total Hamiltonian, describing the interaction of the colliding system with the electromagnetic field. Performing a sequence of two unitary transformations on the wave-function,

$$\psi^{\text{K-H}}(\boldsymbol{r},t) = \hat{U}_{\text{K-H}}\hat{U}_{\text{V}}\psi(\boldsymbol{r},t), \tag{7}$$

one can simplify the TDSE equation, *i.e.* remove the terms $\sim \boldsymbol{A}^2$ and $\boldsymbol{p}\cdot\boldsymbol{A}$. The explicit expressions of $\hat{U}_{\text{V}}$ and $\hat{U}_{\text{K-H}}$ are given in [8]. In the new representation, named after Kramers and Henneberger (see [9] and references therein), the TDSE assumes the form

$$i\hbar\frac{\partial\psi^{\text{K-H}}(\boldsymbol{r},t)}{\partial t} = \left[-\frac{\hbar^2}{2\mu}\nabla_r^2 + V(\boldsymbol{r}+\boldsymbol{\alpha}(t))\right]\psi^{\text{K-H}}(\boldsymbol{r},t), \tag{8}$$

where

$$\boldsymbol{\alpha}(t) = -\frac{eZ_{\mathrm{eff}}}{\mu}\int_{-\infty}^{t}\mathrm{d}t'\boldsymbol{A}(t') = \hat{\boldsymbol{\epsilon}}\alpha_0\sin\omega t \tag{9}$$

is the classical displacement vector of the colliding system center-of-mass from its oscillation center with amplitude

$$\alpha_0 = -eZ_{\mathrm{eff}}\mathcal{E}_0/\mu\omega^2$$

induced by the time-varying electric field $\boldsymbol{E}(t)$. As we argued in [8] this is the *quiver* motion of a charge

$$Z_{\mathrm{eff}} = \frac{Z_1A_2 - Z_2A_1}{A_1+A_2}\,.$$

Note that in the K-H representation the effect of the electromagnetic field is completely transferred into the argument of the scattering potential.

We solve eq. (8) by resorting to the S-matrix formalism [10]. In the absence of the scattering potential the unperturbed wave-functions are

$$\psi_0^{\text{K-H}}(\boldsymbol{r},t) = \Phi_{\boldsymbol{k}}(\boldsymbol{r}) e^{\frac{i}{\hbar}E_k t}, \tag{10}$$

where

$$\Phi_{\boldsymbol{k}}(\boldsymbol{r}) = (2\pi)^{-3/2}\exp(i\boldsymbol{k}\cdot\boldsymbol{r}) \tag{11}$$

are eigenstates of the non-perturbed Hamiltonian $H_0 = -\frac{\hbar^2}{2\mu}\nabla_r^2$. Next, we switch to the interaction representation, such that the perturbed wave-function and the time-dependent scattering potential are transformed to

$$\left|\psi_I{}^{\text{K-H}}\right\rangle = e^{iH_0 t/\hbar}\left|\psi^{\text{K-H}}\right\rangle, \tag{12}$$

$$V_{\text{I}}(t) = e^{iH_0 t/\hbar} V(t) e^{-iH_0 t/\hbar}. \tag{13}$$

Thence the probability amplitude for the transition $\boldsymbol{k}_i \longrightarrow \boldsymbol{k}_f$ during the collision is casted in the form [10]

$$C_{\boldsymbol{k}_i,\boldsymbol{k}_f}(t) = \langle\Phi_{\boldsymbol{k}_f}|\mathcal{T}\exp\left[-\frac{i}{\hbar}\int_0^t \mathrm{d}t\, V_{\text{I}}(\boldsymbol{r}+\boldsymbol{\alpha}(t))\right]|\Phi_{\boldsymbol{k}_i}\rangle, \tag{14}$$

where $\mathcal{T}$ is the Dyson time-ordering operator. For instance, when acting on the product of two operators which are function of time, $\mathcal{T}$ moves the operator involving an earlier time to the right. If the limits of integration over time in eq. (14) are extended to $t = -\infty$ for the initial time and $t = +\infty$ for the final time, the transition probability amplitude after the collision is denoted by the matrix element of the S-matrix

$$C_{\boldsymbol{k}_i,\boldsymbol{k}_f}(\infty) = \langle\Phi_{\boldsymbol{k}_f}|\hat{S}|\Phi_{\boldsymbol{k}_i}\rangle. \tag{15}$$

A series expansion of the exponential in eq. (14) in powers of $V_{\text{I}}(t)$ provides the Born series. The first Born approximation reads

$$\begin{aligned} S_{fi}^{\text{B}} &= S_{fi}^{(0)} + S_{fi}^{(1)} \\ &= \delta(\boldsymbol{k}_f - \boldsymbol{k}_i) + \frac{1}{i\hbar}\langle\Phi_{\boldsymbol{k}_f}|\int_{-\infty}^{+\infty}\mathrm{d}t V_{\text{I}}(\boldsymbol{r}+\boldsymbol{\alpha}(t))|\Phi_{\boldsymbol{k}_i}\rangle. \end{aligned} \tag{16}$$

The above matrix element can be worked out by introducing the Fourier transform of the scattering potential in the K-H representation, *i.e.*

$$V(\boldsymbol{r}+\boldsymbol{\alpha}(t)) = \int \mathrm{d}\boldsymbol{q}\widetilde{V}(\boldsymbol{q})\exp[-i\boldsymbol{q}\cdot(\boldsymbol{r}+\boldsymbol{\alpha}(t))] \tag{17}$$

and the generating function of the Bessel function of integer order [11]

$$e^{-i\Delta\boldsymbol{q}\cdot\boldsymbol{\alpha}(t)} = \sum_{n=-\infty}^{\infty} J_n(\Delta\boldsymbol{q}\cdot\hat{\boldsymbol{\epsilon}}\alpha_0)e^{-in\omega t}. \tag{18}$$

We obtain after some mathematical manipulations the first-order matrix element

$$\begin{aligned} S_{fi}^{(1)} &\equiv \langle\Phi_{\boldsymbol{k}_f}|\int_{-\infty}^{+\infty}\mathrm{d}t\, V_{\text{I}}(\boldsymbol{r}+\boldsymbol{\alpha}(t))|\Phi_{\boldsymbol{k}_i}\rangle \\ &= -2\pi i\widetilde{V}(\boldsymbol{q})\sum_{n=-\infty}^{\infty} J_n(\Delta\boldsymbol{q}\cdot\hat{\boldsymbol{\epsilon}}\alpha_0)\delta(E_{k_f} - E_{k_i} - n\hbar\omega). \end{aligned} \tag{19}$$

In the above formulas $\boldsymbol{k}_{i,f}$ are the initial and final momenta of the colliding system in the C.M. Their absolute values are

$$k_i = \left(\frac{2\mu}{\hbar^2}E_{k_i}\right)^{1/2}, \qquad k_f = \left(\frac{2\mu}{\hbar^2}(E_{k_i} + n\hbar\omega)\right)^{1/2}. \tag{20}$$

We introduced also the momentum transfer during the collision

$$\Delta\boldsymbol{q} = \boldsymbol{k}_i - \boldsymbol{k}_f. \tag{21}$$

The corresponding energy balance is encoded in the delta function $\delta(E_{k_f} - E_{k_i} - n\hbar\omega)$ appearing in eq. (19)

$$E_{k_f} = E_{k_i} + n\hbar\omega, \tag{22}$$

with $n = 0, \pm1, \pm2, \ldots$. Positive values ($n > 0$) signify absorption (stimulated bremsstrahlung), thus $E_{k_f} > E_{k_i}$, whereas negative values ($n < 0$) emission (bremsstrahlung). In this last case the number of emitted photons in the presence of the laser field has a limiting value, *i.e.*,

$$-n \leq \frac{E_{k_i}}{\hbar\omega}. \tag{23}$$

Within the conventional scattering theory [12] the S-matrix is related to the transition (T) matrix element

$$\hat{S} = \hat{I} - 2\pi i\hat{T}. \tag{24}$$

We therefore introduce the Born approximation for the T-matrix of the scattering process accompanied by the exchange of n photons

$$T_{fi}^{\text{B}}(n) = J_n(\Delta\boldsymbol{q}\cdot\hat{\boldsymbol{\epsilon}}\alpha_0)\widetilde{V}(\boldsymbol{q}). \tag{25}$$

Then, in a manner completely analogous to the field-free case [12], the elastic differential cross section for the nucleus-nucleus scattering, accompanied by the absorption (emission) of n photons, is given by

$$\frac{\mathrm{d}\sigma_n}{\mathrm{d}\Omega} = \frac{k_f}{k_i}\left(\frac{\mu}{2\pi\hbar^2}\right)^2\left|T_{fi}^{\text{B}}(n)\right|^2. \tag{26}$$

Consequently the differential cross section for laser-assisted nucleus-nucleus scattering is given in the first-Born approximation (derived in this form for the first time by Bunkin and Fedorov [2]) by

$$\frac{\mathrm{d}\sigma_n}{\mathrm{d}\Omega} = \frac{k_f}{k_i}J_n^2(\Delta\boldsymbol{q}\cdot\boldsymbol{\alpha}_0)\left(\frac{\mathrm{d}\sigma}{\mathrm{d}\Omega}\right)_{\text{B1}}(\Delta\boldsymbol{q}), \tag{27}$$

Table 1. Unique solution with WS[1] and WS[2] form factors for the reaction ^{4}He + ^{58}Ni at 139 MeV. Standard notations for the optical potential parameters are used. In our analysis the best χ^2 is calculated with 10% error at all experimental points.

	V	W	r_V	r_W	r_c	a_V	a_W	χ^2	σ_R	J_V	R_V	J_W	R_W
	MeV	MeV	fm	fm	fm	fm	fm		mb	MeV · fm^3	fm	MeV · fm^3	fm
WS[1]	111.	20.16	0.9200	1.1700	1.0	0.7830	0.5350	1.53	1664.	315.	4.8580	101.	5.3314
WS[2]	158.	19.90	0.9464	1.2620	1.0	1.4078	1.0909	1.47	1722.	284.	4.7198	86.	5.4376

where

$$\left(\frac{\mathrm{d}\sigma}{\mathrm{d}\Omega}\right)_{\mathrm{B1}}(\Delta\boldsymbol{q}) = \left(\frac{\mu}{2\pi\hbar^2}\right)^2 \left|\widetilde{V}(\boldsymbol{q})\right|^2 \tag{28}$$

is the field-free elastic scattering differential cross section in the first Born approximation. As can be seen in eq. (27) the differential cross section depends, via the argument of the Bessel function, on the orientation of the polarization vector $\hat{\boldsymbol{\epsilon}}$ relative to $\Delta\boldsymbol{q}$. Thus, the effect of the laser fields enters the expression (27) via the square of the Bessel function $J_n^2(\Delta\boldsymbol{q}\cdot\boldsymbol{\alpha}_0)$.

It is worthwhile to comment on the case when there is a huge discrepancy in magnitude between the collision energy and the energy of exchanged photons, *i.e.* $E_{k_i} \gg n\hbar\omega$. Since in this case $k_f \approx k_i$, summing eq. (27) after the photon number, such that always $k_f \geq 0$, and using the addition theorem for the Bessel function of integer order (9.1.76 of [11])

$$1 = \sum_n J_n^2(\Delta\boldsymbol{q}\cdot\boldsymbol{\alpha}_0) \tag{29}$$

the following sum rule is fulfilled:

$$\sum_n \frac{\mathrm{d}\sigma_n}{\mathrm{d}\Omega} \approx \left(\frac{\mathrm{d}\sigma}{\mathrm{d}\Omega}\right)_{\mathrm{B1}}. \tag{30}$$

A last comment that we would like to make in this section concerns the range of applicability of eq. (27). Although this issue was never rigorously investigated, as mentioned in ref. [2], a condition leading to eq. (27) is that the laser frequency is small compared to the bombarding energy, *i.e.*

$$\xi = \frac{\hbar\omega}{2E_{k_i}} \ll 1. \tag{31}$$

At the highest photon energy considered in this paper, $\xi \approx 5\times10^{-8}$.

3 Elastic scattering of ^{4}He + ^{58}Ni at 139 MeV

3.1 Field-free scattering

The reaction ^{4}He + ^{58}Ni at 139 MeV has been measured by Goldberg *et al.* [13] in an effort to clarify the problem of discrete ambiguities which for long time hampered the heavy-ion elastic scattering studies at low energies. Besides the strong evidence for refractive effects, the analysis of this reaction showed a way to eliminate most of the discrete potentials. The authors conjectured that phase

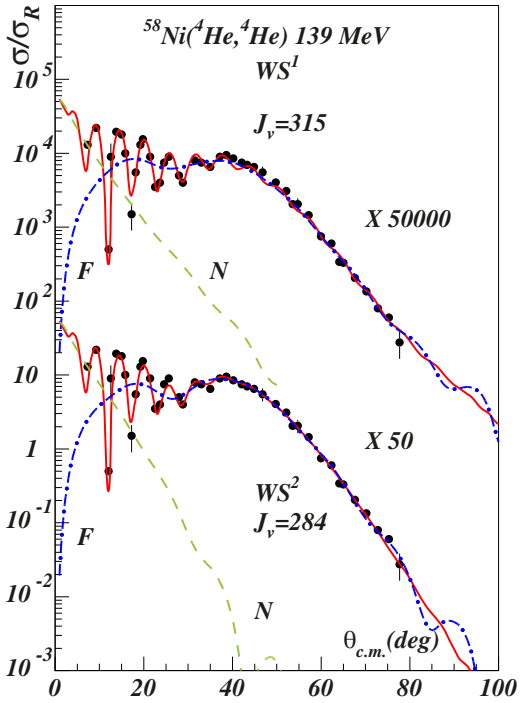

Fig. 1. F/N decomposition with WS[1] and WS[2] form factors for the typical rainbow scattering of ^{4}He on ^{58}Ni at a laboratory energy $E = 139$ MeV.

equivalence of discrete potentials disappear if and only if the incident energy is high enough such that a rainbow develops and there are sufficient measured data points in the dark side of the rainbow. The critical energy is defined as the incident energy for which the effective potential has an inflection point instead of a pocket for a specific angular momentum. The conjecture was checked substantially for reactions on light and medium mass nuclei at 104 MeV [14] and in the Nickel region at 172.5 MeV [15].

Since the finding of the optical potential is the royal route to wave functions and nuclear structure, we describe below in some details a standard optical model analysis in an effort to reveal the reaction mechanism governing the reaction and to guide the reader for future laser assisted experiments. A grid search using standard Woods-Saxon (WS[1] and WS[2]) form-factors including volume absorption and supplemented with hard sphere Coulomb potentials revealed a unique solution (see table 1 and fig. 1). These solutions have moderate values for imaginary volume integrals and real volume integrals close to the critical value $J_V \approx 300$ MeV fm^3, which ensures strong refractive effects. The calculated angular distributions displayed in

fig. 1 show a typical rainbow pattern with large amplitude diffractive Fraunhofer oscillations at forward angles followed by a rainbow hump and exponential decay at large angles. The dominating farside component (F) shows a hint of an Airy oscillation forward to the rainbow hump while the nearside component (N) exponentially decays after the Fraunhofer crossover. The uniqueness of the solution is guaranteed by the huge parameter space which has been explored in the search procedure.

The ability of semi-microscopic folding potentials to describe rainbow scattering was tested by many authors, see *e.g.* [15]. We use here a scaling procedure initially introduced by Mahaux *et al.* [16] which ensures a high flexibility of the folding form factors. In the folding model, the spin-isospin independent form factor of the optical potential is given by the integral

$$V_{\rm fold}(\boldsymbol{R}) = \int {\rm d}\boldsymbol{r}_1 {\rm d}\boldsymbol{r}_2 \rho_1(\boldsymbol{r}_1)\rho_2(\boldsymbol{r}_2) v_{\rm eff}(\boldsymbol{s}), \qquad (32)$$

where $v_{\rm eff}$ stands for a density dependent G-matrix interaction, $\rho_{1,2}$ are the Hartree-Fock single-particle spherical densities of the projectile and target, and $\boldsymbol{s} = \boldsymbol{r}_1 + \boldsymbol{R} - \boldsymbol{r}_2$ is the NN (nucleon-nucleon) separation distance in a standard double folding geometry. We use the well known D1N parametrization of the Gogny [17] effective interaction as well as the nuclear matter approach of Jeukenne, Lejeune and Mahaux (JLM) [16] which incorporates a complex energy and density dependent parametrization of the NN interaction obtained in a Brueckner-Hartree-Fock approximation from the Reid soft core NN potential. We note that the nonlocal knock-on exchange kernel of the Gogny interaction is localized using the lowest order of the Perey-Saxon approximation [18]. We keep the number of fitting parameters at the minimum level and take the optical potential in the form

$$U(R) = N_V V(R, t_V) + i N_W V(R, t_W), \qquad (33)$$

where $N_{V,W}$ are normalization constants and $t_{V,W}$ are range parameters defined by the scaling transformation,

$$V(R, t) \rightarrow t^3 V_{\rm fold}(tR). \qquad (34)$$

This transformation conserves the volume integral of the folding potential and modifies the radius as

$$\langle R^2 \rangle_V = \frac{1}{t^2} \langle R^2 \rangle_{\rm fold}. \qquad (35)$$

Thus the strength of the form factor is controlled by the normalization parameters $N_{V,W}$. The effective mass correction [19], $\mu^*/\mu = 1 - \partial U/\partial E$ is of the order of a few percent for our system and is absorbed in the renormalization parameter N_W. Note that the transformation in eq. (34) ensures that only the *rms* radius of the bare folding potential is changed. This is in line with the original prescription of [16] which proposed a smearing procedure in terms of a normalized Gaussian function. We found that the transformation in eq. (34) is more efficient and less time consuming. Based on eq. (35) one may estimate in an average way the importance of the dynamic polarization potential (DPP) and finite range effects. In the present analysis we use single particle densities obtained from a spherical Hartree-Fock (HF+BCS) calculation based on the density functional of Beiner and Lombard [20] for which the real range parameter of the folding potential requires only a few-percent correction. The obtained *rms* charge radii are very close to the experimental values [21]. The effective interactions are density dependent and therefore two approximations were used for the overlap density,

$$\rho = \sqrt{\rho_1(r_1)\rho_2(r_2)} \qquad (36)$$

and

$$\rho = \frac{1}{2}(\rho_1(r_1) + \rho_2(r_2)). \qquad (37)$$

Though both approximations lead to the same volume and *rms* radii, the first one, *i.e.* (36) has the advantage over (37) in that it insures the vanishing of the overlap density once one of the interacting nucleons is far from the bulk. In eq. (37) a factor 1/2 was introduced such that the overlap density does not exceeds the equilibrium density for normal nuclear matter. At large density overlaps, the fusion and other inelastic processes are dominant and the elastic scattering amplitude is negligible small.

The calculated OM potentials are dubbed GOGNY1 (corresponding to approximation (36)) and GOGNY3 (for (37)) and similarly for the JLM interaction: JLM1 and JLM3. Both definitions represent crude approximations of the overlap density but are widely used in the estimation of the density dependence effects in the folding model. The bulk parameters collected in table 2 (volume integrals, *rms* radii and total reaction cross section), which are the most pertinent physical observables which can be extracted from elastic angular distributions show that there is little difference between eqs. (36) and (37) since both lead to almost identical values. We mention that we first introduced the interaction GOGNY1 in refs. [22,23] where we described consistently the hindrance in sub-barrier fusion of several reacting systems with ^{40,48}Ca projectiles.

A unique solution is also obtained with the folding model (see table 2). The calculated angular distributions (normalized to the Rutherford cross section), supplemented by a standard farside/nearside (F/N) decomposition are shown in fig. 2. The calculation is completely consistent with the previous Woods-Saxon (WS) calculation, showing a well defined Fraunhofer sector followed by a rainbow hump and an exponential decay at large angles. The bulk observables (volume integral, *rms* radii and total reaction cross section) are also consistent.

We should note that the farside dominance in our angular distribution suggests strong refractive effects such as rainbows, but the F/N decomposition is not sufficient to completely clarify the reaction mechanism. The reason for such a behavior is that the F/N method does not perform a dynamic decomposition of the scattering function, but merely decomposes the scattering amplitude into traveling waves. A useful dynamic decomposition of the S-matrix can be obtained with the semiclassical method of Brink and Takigawa [24]. This method uses classical ingredients

Table 2. Unique solutions with folding form factors for the reaction $^4\mathrm{He} + {}^{58}\mathrm{Ni}$ at 139 MeV.

	N_V	N_W	t_V	t_W	χ^2	σ_R	J_V	R_V	J_W	R_W
						mb	MeV · fm^3	fm	MeV · fm^3	fm
GOGNY1	0.545	0.2059	1.0030	0.8943	2.91	1743.	274.24	4.674	102.98	5.235
GOGNY3	0.725	0.2794	1.0203	0.9174	3.82	1731.	275.70	4.679	105.65	5.197
JLM1	0.620	0.6752	0.9430	0.8577	1.94	1745.	277.98	4.670	100.16	5.270
JLM3	0.665	0.7665	0.9387	0.8558	2.09	1752.	276.60	4.684	99.43	5.297

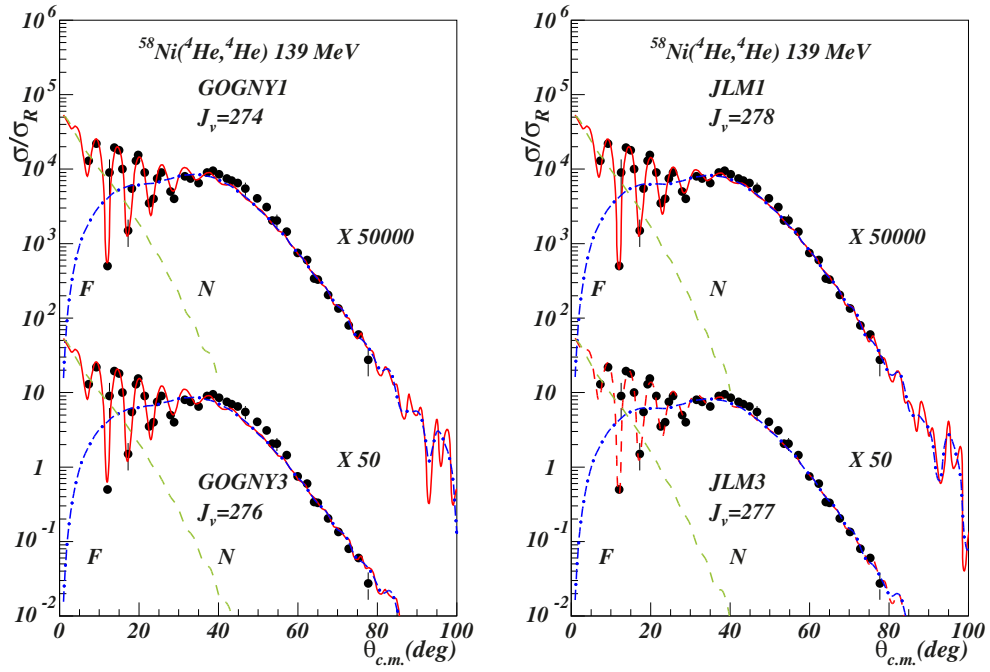

Fig. 2. Same as in fig. 1 with GOGNY form factors (left panel) and with JLM form factors (right panel).

such as complex turning points, action integrals and potential poles to decompose the scattering amplitude into barrier and internal barrier subcomponents. The barrier (B) component accounts for the particle flux reflected at the most external barrier complex turning point, while the internal barrier (I) component describes the waves penetrating the barrier, suffering multiple reflexions between the internal turning points and thus exploring the potential in the interior sector. When this latter component is large, a palette of exotic phenomena may appear in heavy ion elastic angular distribution such as nuclear orbiting and rainbows.

3.2 Scattering in a linearly polarized radiation field

3.2.1 Continuous-wave signals

We consider the simplest possible charged particle scattering experiment in the presence of a spatially homogeneous laser field and polarization $\hat{\boldsymbol{\epsilon}}$ along the beam direction ($\hat{\boldsymbol{\epsilon}} \parallel \boldsymbol{k}_i$) and for an infinite pulse duration

$$\boldsymbol{E}(t) = \hat{\boldsymbol{\epsilon}}\mathcal{E}_0 \sin \omega t. \tag{38}$$

In other words, the above Ansatz is justified for a *gedanken* experiment of field-assisted potential scattering, where the projectile-target reaction takes place in a domain with linear size $\ll \lambda$.

We consider the reaction $^4\mathrm{He} + {}^{58}\mathrm{Ni}$ at 139 MeV and assume that the theory outlined in refs. [1,2], whose main result was given in eq. (27), can be applied in this case. We note that the sum rule, written above, *e.g.* (30), in the first Born approximation, was proven by Kroll and Watson to be valid to all orders within the low-frequency approximation (LFA) [1].

$$\sum_n \mathrm{d}\sigma_n = \mathrm{d}\sigma_{\mathrm{el}}. \tag{39}$$

In view of the huge discrepancy between the laser photon energy $\hbar\omega$ and the collision energy E, we expect this approximation to be valid. Since for the geometry assumed

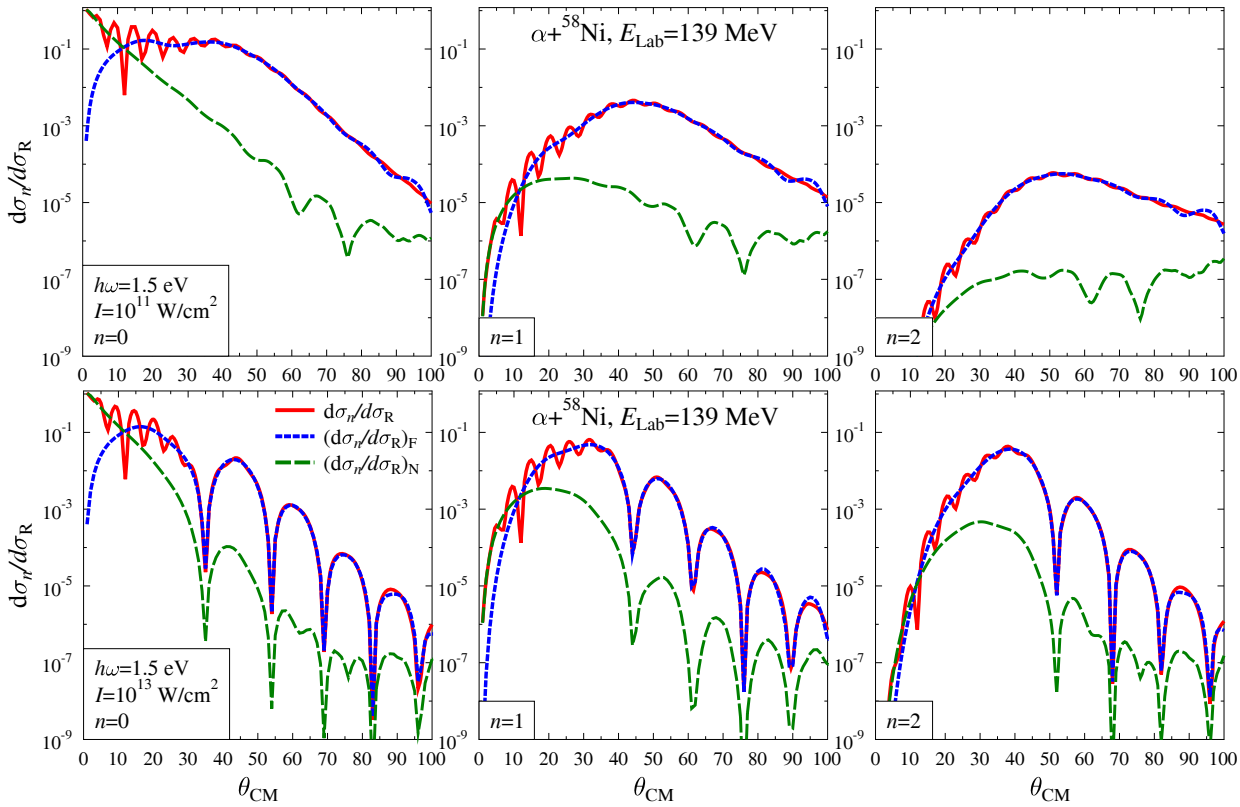

Fig. 3. Elastic scattering $^4\mathrm{He} + {}^{58}\mathrm{Ni}$ at 139 MeV assisted by a laser field with photon energy $\hbar\omega = 1.5\,\mathrm{eV}$ for two intensities: $I = 10^{11}\,\mathrm{W/cm^2}$ (top panels) and $I = 10^{13}\,\mathrm{W/cm^2}$ (bottom panels). $\mathrm{d}\sigma_n/\mathrm{d}\sigma_R$ is calculated for $n = 0$, $n = 1$ and $n = 2$ absorbed photons. The F/N decomposition is figured by the short-dashed curve (farside) and the long-dashed curve (nearside).

above $\Delta\boldsymbol{q}\cdot\hat{\boldsymbol{\epsilon}} = 2k_i\sin^2\theta_{\mathrm{c.m.}}/2$, where $\theta_{\mathrm{c.m.}}$ is the center of mass scattering angle, the differential cross-section (27) for non-relativistic laser-assisted ion-ion scattering, corresponding to the emission or absorption of n photons in the case analyzed in this section, is rewritten as

$$\left(\frac{\mathrm{d}\sigma_{\pm n}}{\mathrm{d}\Omega}\right)_{\mathrm{LFA}} = \frac{k_f(\pm n)}{k_i} J_n^2(\zeta_i(\theta)) \left(\frac{\mathrm{d}\sigma}{\mathrm{d}\Omega}\right)_{\mathrm{el}}, \qquad (40)$$

where $\zeta_i = 2\alpha_0 k_i \sin^2(\theta_{\mathrm{c.m.}}/2)$.

We note in passing that the relation between the electric field strength $\mathcal{E}_0$ and the laser intensity $I_0 = \frac{1}{2}c\epsilon_0\mathcal{E}_0^2$ can be recasted for practical purposes as [25]

$$\mathcal{E}_0[\mathrm{V/cm}] = 27.44\left\{I_0[\mathrm{W/cm^2}]\right\}^{1/2}.$$

It is expected that the 2 lasers of ELI-NP, each endowed with a power of 10 PW power, will produce a maximum intensity $I_0 \approx 10^{23}\,\mathrm{W/cm^2}$ [26]. The corresponding electric field is $\mathcal{E}_0 \approx 8.7\times10^{12}\,\mathrm{V/cm}$ or, in nuclear units, using the amplitude of the electric force on the elementary charge $+e$

$$e\mathcal{E}_0 \approx 8.7\times10^{-7}\,\mathrm{MeV/fm}.$$

For the numerical examples presented below we take values that do not exceed $e\mathcal{E}_0 \approx 8.7\times10^{-10}\,\mathrm{MeV/fm}$. First we consider the case of Ti:sapphire laser beam $\hbar\omega = 1.5\,\mathrm{eV}$ impinging on the projectile beam and the target, as well as higher photon energies that are currently unavailable, just for the sake of assessing the role played by the photon frequency.

In fig. 3 we display the laser-assisted cross-section in ratio to Rutherford cross section ($\mathrm{d}\sigma_n/\mathrm{d}\sigma_R$) as well as its F/N decomposition (total, far- and nearside) in the photonless case ($n = 0$) and for the absorption of $n = 1$ and $n = 2$ photons for two moderate intensities ($I = 10^{11}$ and $10^{13}\,\mathrm{W/cm^2}$). The unperturbed cross section is calculated with a strongly refractive WS[1] solution. Large amplitude oscillations are superimposed on the rainbow exponential decay of the cross section at the larger intensity. The Fraunhofer characteristic oscillations are still visible in the forward angle sector, despite the behavior of the Bessel function for small arguments. At large angles, both farside and nearside components of the cross-section display strong oscillations for the higher intensity. Instead, at the lower intensity the same quantity for $n = 0$ resembles the unperturbed case. By symmetry, the case of photon emission by heavy ions is identical to the absorption case.

One of the most stringent effects produced by the exchange of photons between the projectile-target system and the electromagnetic fields is manifested by the drastically depletion of the cross section for small angles when $n \neq 0$. By comparing with fig. 2 we see that the nearside component suffers a dramatic change in behavior for

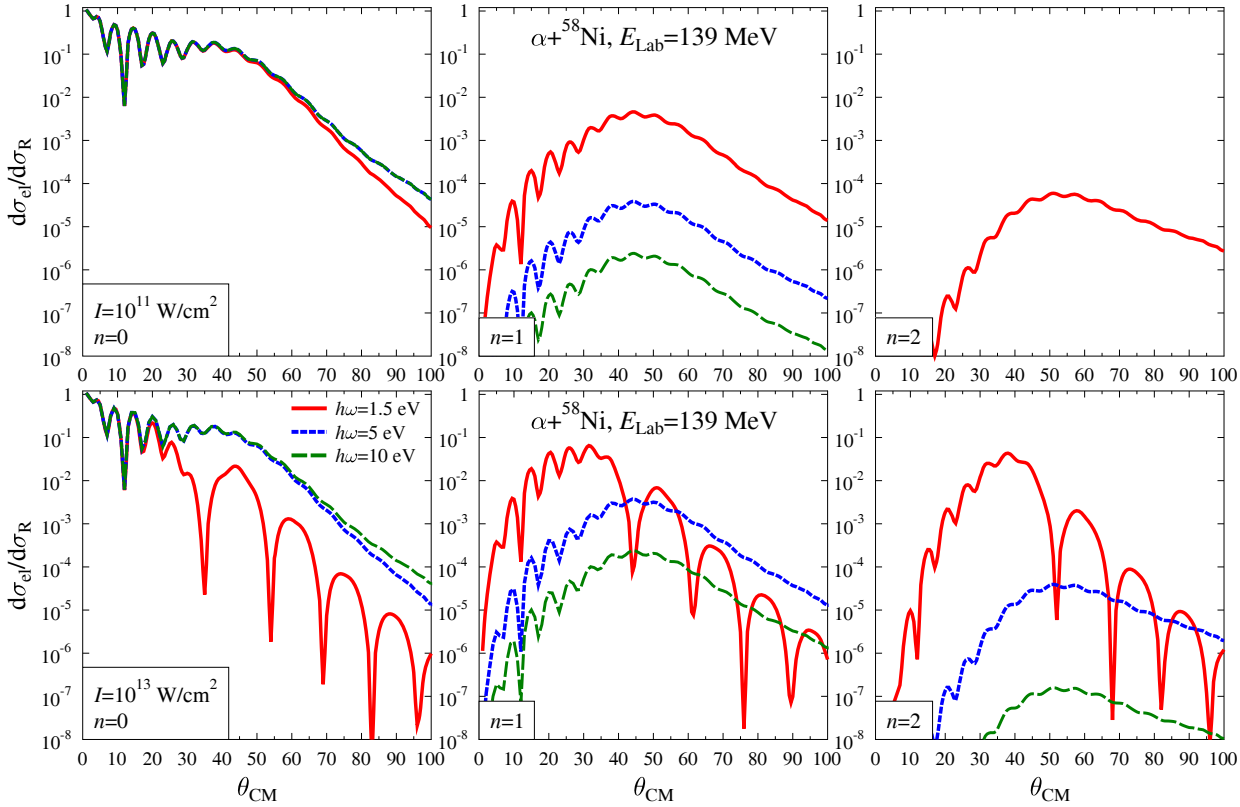

Fig. 4. Elastic scattering $^4\mathrm{He} + {}^{58}\mathrm{Ni}$ at 139 MeV assisted by a laser field with photon energies $\hbar\omega = 1.5\,\mathrm{eV}$, 5 eV, 10 eV and for two intensities: $I = 10^{11}\,\mathrm{W/cm^2}$ (top panels) and $I = 10^{13}\,\mathrm{W/cm^2}$ (bottom panels). $\mathrm{d}\sigma_n/\mathrm{d}\sigma_R$ is calculated for $n = 0$, $n = 1$ and $n = 2$ absorbed photons.

small angles. Instead, the farside component, though it also shrinks in the forward direction, preserves its monotonically increasing shape in this region. The rainbow hump is damped by several orders of magnitude at the lower intensity for $n \neq 0$. However, when passing from the lower to the higher intensity, the broad rainbow hump in the field-free case displays a fragmentation in several oscillations with decreasing amplitude and is shifted towards larger angles with increasing n. On the other hand, the slope of the cross-section at the higher intensity is nearly the same for $n = 0, 1$ and 2 exchanged photons.

We also turned our attention to lasers of lower wavelength that are in the upper range of the ultraviolet radiation. The numerical experiments that we performed for higher photon energies and displayed in fig. 4 are pointing to a drop of the cross-section by orders of magnitude with the number of exchanged photons n and for increasing photon energy $\hbar\omega$ at the lowest intensity. This suppresion is related to the behavior of the Bessel function for small values of the argument, *i.e.* $J_n(x) \sim (x/2)^n/n!$ [11]. In the absence of photon exchange the cross-section for the two higher photon energies barely change with increasing intensity. For the real laser ($\hbar\omega = 1.5\,\mathrm{eV}$) the argument of the Bessel function J_0 is larger by a factor of 11.1 and 44.4 respectively compared to the other two higher frequencies! It is transparent from this discussion that at higher photon energies the argument of the Bessel function decreases $\sim 1/\omega^2$ which has the effect to compensate the linear increase in the field strength (compare for example the $\hbar\omega = 5\,\mathrm{eV}$ curve at higher intensity with the $\hbar\omega = 1.5\,\mathrm{eV}$ at the lower intensity for $n = 0$ in fig. 4).

In fig. 5 we investigate the effect of large numbers of absorbed photon, for increasing laser intensity and a selection of 4 photon energies. For the lowest intensity only the photonless events contribute to the cross-section in the course of the reciprocal diffraction laser-heavy ions. For the highest intensity the contribution of $n \neq 0$ strengths is dramatically pushed up. As we already remarked in the previous figure, the exchange of numerous photons is favored for the lowest photon energy! At the highest intensity the maximum of the strength distribution lays at $n = 4$.

3.2.2 Pulsed signals

For shorter laser pulses (ultra-short pulses lasting few optical cycles), the electromagnetic wave can be formed by superimposing monochromatic plane waves. For non-dispersive, linearly polarized laser pulses, the vector potential is casted in the form [27]

$$\boldsymbol{A}(\boldsymbol{r}, t) = -\hat{\boldsymbol{\epsilon}}\mathcal{E}_0 \int_{-\infty}^{t} F(t' - \boldsymbol{k}\cdot\boldsymbol{r}/\omega)\sin(\omega t' - \boldsymbol{k}\cdot\boldsymbol{r})\mathrm{d}t', \tag{41}$$

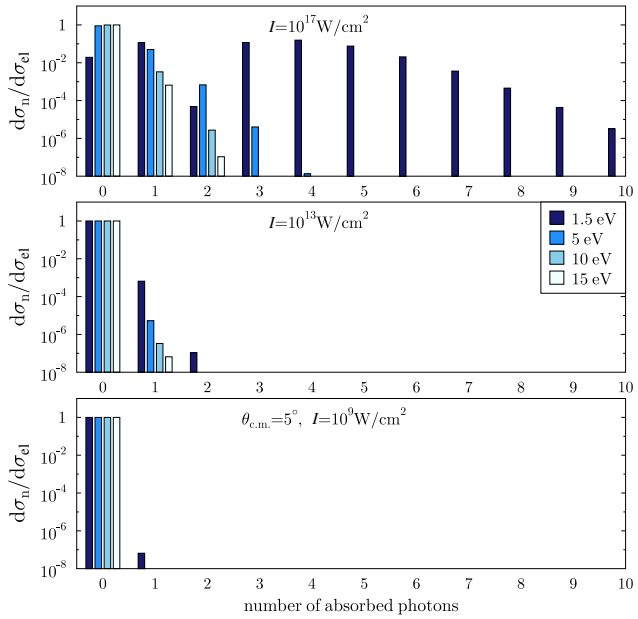

Fig. 5. The n-photon differential cross section as a function of the number of absorbed photons for three laser intensities ($I = 10^9$, 10^{13} and $10^{17}\,\mathrm{W/cm^2}$) and fixed scattering angle ($\theta = 5°$). For each intensity we represent the strength at four photon energies ($\hbar\omega = 1.5, 5, 10$ and $15\,\mathrm{eV}$). The scattering angle has been chosen arbitrarily at $\theta = 5°$ in the Fraunhofer sector of the field-free scattering.

where $\hat{\boldsymbol{\epsilon}}$ is the polarization vector, $\mathcal{E}_0 = \omega A_0$ is the amplitude of the electric field and F is a non-negative function that describes the shape (envelope) of the pulse. In the dipole approximation the vector potential satisfies the Coulomb gauge, $\boldsymbol{\nabla}\cdot\boldsymbol{A} = 0$, and with no sources present, the electric field of the laser pulse is

$$\boldsymbol{E} = -\frac{\partial A}{\partial t} = \hat{\boldsymbol{\epsilon}}\mathcal{E}_0 F(t - \boldsymbol{k}\cdot\boldsymbol{r}/\omega)\sin(\omega t - \boldsymbol{k}\cdot\boldsymbol{r}). \tag{42}$$

In the dipole approximation the electric field of a linearly polarized laser pulse is

$$\boldsymbol{E}(t) = \hat{\boldsymbol{\epsilon}}\mathcal{E}_0 F(t)\sin(\omega t). \tag{43}$$

In this paper we introduce the pulse duration τ_p as the full width at half maximum of the intensity profile $|\boldsymbol{E}(t)|^2$. Further, we consider three types of envelopes that are commonly encountered in the literature [28] with the following profiles:

rectangular (step function)

$$F(t) = \Theta(\tau_p - t), \tag{44}$$

sine-squared

$$F(t) = \sin^2\left(\frac{\pi t}{\tau_p}\right)\Theta(\tau_p - t), \tag{45}$$

and Gaussian

$$F(t) = \exp\left[-4\pi^2 t^2/\tau_p^2\right]\Theta(\tau_p - t). \tag{46}$$

The pulse duration is taken in our study as an integer multiple of the laser period, *i.e.* $\tau_p = NT$. Although for these pulses the minimum N is about a few dozens of cycles, we find instructive for our study to consider pulse lengths of a few cycles.

In order to adapt the K-W theorem (27) to the case of laser pulses of finite duration we appeal to a suggestion made long time ago by Krüger and Jung [29]. It is assumed that the shape function $F(t)$ varies so slowly with t, that for time intervals long compared to $1/\omega$, it can be approximated piecewise to a good accuracy by the sum

$$F(t) = \sum_{p=1}^{N} f_p[\Theta(T_p - t) - \Theta(T_{p-1} - t)], \tag{47}$$

where

$$f_p = F\left(\frac{T_{p-1} + T_p}{2}\right). \tag{48}$$

Then the differential cross section for n-photons exchanged is obtained as a time average over the interval $[T_0, T_N]$ of length $\tau_p = T_N - T_0$

$$\frac{\mathrm{d}\bar{\sigma}_n}{\mathrm{d}\Omega} = \frac{1}{\tau_p}\int_{T_0}^{T_N} \mathrm{d}t \frac{\mathrm{d}\sigma_n(F(t))}{\mathrm{d}\Omega}, \tag{49}$$

where $(\mathrm{d}\sigma_n(F(t))/\mathrm{d}\Omega)$ is calculated for $F(t) = f_p$. In other words,

$$\frac{\mathrm{d}\bar{\sigma}_n}{\mathrm{d}\Omega} \approx \frac{k_f}{k_i}\left(\frac{\mathrm{d}\sigma}{\mathrm{d}\Omega}\right)_{\rm elast}\frac{1}{\tau_p}\int_{T_0}^{T_n} \mathrm{d}t J_n^2(\boldsymbol{k}\cdot\boldsymbol{\alpha}_0(t)) \tag{50}$$

where

$$\alpha_0(t) = -\frac{eZ_{\rm eff} f_p \mathcal{E}_0}{\mu\omega^2}[\Theta(t - T_{p-1}) - \Theta(T_p - t)]. \tag{51}$$

In fig. 6 the strengths (50) are displayed for the three modulated signals discussed above with pulse duration $\tau_p = 2\pi/\omega$ and the highest intensity used in the present study. The dependence of the strengths on the shape of the chosen modulated pulse is striking. For the Gaussian pulse, the strength drops fast with n and consequently the "multiphoton" contributions are manifest for the square pulse up to $n = 4$. The strengths for the sine-squared pulse display a behavior closer to the rectangular pulse.

In fig. 7 we plot the same quantity like in fig. 6, this time only for the Gaussian pulse and for finite pulse durations ($\tau_p = T, 3T$ and $5T$). By increasing τ_p, the exchange of photons is enhanced.

4 Summary and outlook

In this study we considered the elastic scattering of two nuclei in the presence of a monochromatic laser field. This is one of the few elementary processes where the description of the assisting radiation field may be non-perturbatively incorporated into the theory. This opens

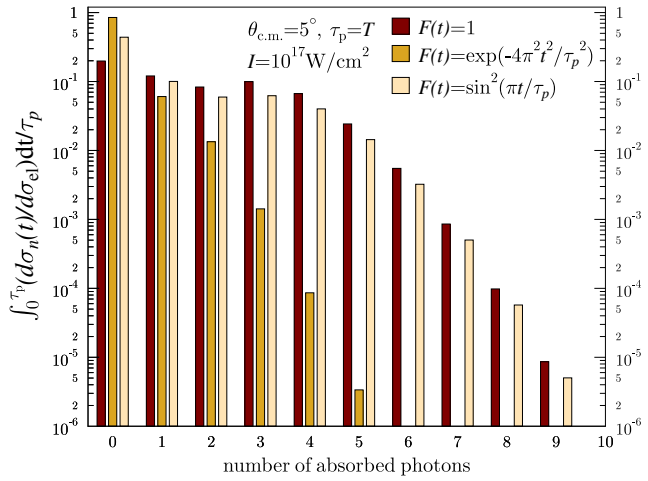

Fig. 6. The time-average of the n-photon differential cross section (49) over the pulse duration τ_p as a function of the number of absorbed photons for three envelopes of the electric field $F(t)$ (square, Gaussian and sine-squared), laser pulse intensity $I = 10^{17}\,\mathrm{W/cm^2}$ and fixed scattering angle ($\theta = 5°$) for the Ti:sapphire laser. The duration of the pulse is one light period T.

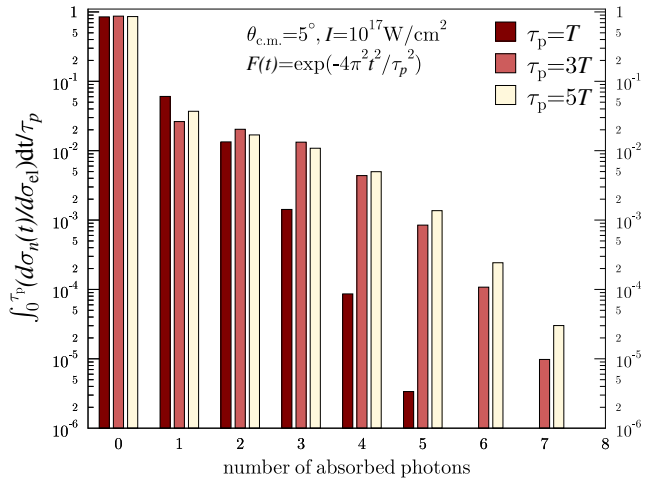

Fig. 7. The time-average of the n-photon differential cross section (49) over the pulse duration τ_p as a function of the number of absorbed photons, for a Gaussian envelope and intensity $I = 10^{17}\,\mathrm{W/cm^2}$ at fixed scattering angle ($\theta = 5°$) for the Ti:sapphire laser. We take three pulse durations: $\tau_p = T, 3T$ and $5T$.

the possibility of studying in a rather simple way strong-field effects and multiphoton processes in nuclear systems.

We have chosen as an example a typical heavy-ion reaction, where the field-free cross-section displays a superposition of diffractive Fraunhofer and refractive (rainbow) scattering regimes. Using the standard optical model framework, accompanied by a detailed semiclassical (WKB) analysis, we clarified the reaction mechanism before embarking to a detailed investigation of the dependence of the shape and amplitude of the cross-section. The numerical experiments were performed for several parameters of the laser field impinging on the heavy ions, *i.e.* intensity I, photon frequency ω, as well as the role of multiphoton processes, shape and duration of modulating laser pulses.

Along with the optical Ti:sapphire laser ($\lambda = 800\,\mathrm{nm}$) we also assumed photons of lower wavelengths produced by a fictitious laser, though not far beyond the technical possibilities foreseen in the near future. Already laser facilities around the globe are able to produce beams of ultraviolet and X-ray lasers. By no means we intended to venture in the realm of speculations and academic exercises, rather we aimed to validate possible paths of research in laser assisted nuclear reactions.

The diffraction pattern of heavy ions in the laser field accompanied by the exchange of one or more photons is characterized by a drastic reduction of the quantum scattering flux in the forward direction.

Multiphoton effects seem to be favored provided a relatively moderate laser intensity $I = 10^{17}\,\mathrm{W/cm^2}$ is attained. However, the possibility to observe such events is severely hampered by the corresponding reduction of the cross-section.

On the other hand there are still many questions not discussed in this paper. We considered the scattering of two nuclei in the field of a linearly polarized, monochromatic, homogeneous laser field (see eq. (38)). In a more realistic treatment the colliding nuclei are found in regions of different field strengths. In this case one has to take into account the effects of an intensity variation of the field not only in time, but also in space. The laser beam can be described by a plane-wave of the type given in eq. (1) modulated by a slowly space varying function [30]. In preparing an experiment there are several facts that need to be taken into account. The effective range of the nucleus-nucleus of the potential, despite its Coulomb nature, is small compared to the laser wavelength and therefore also small compared to the spatial variations of the intensity. However, due to the extension of the target, as discussed above, the spatial variations of the field across the target have to be accounted for. In practice each space-time point $(\boldsymbol{r}, t)$ should be weighted by $n(\boldsymbol{r}, t)$, the density of nucleus-nucleus collision events. Consequently the detector counting these events in an experiment carried out with a space and time-dependent field intensity will eventually provide a total number of observed events proportional to the differential cross-section (40) multiplied by $n(\boldsymbol{r}, t)$ and integrated over the macroscopic interaction volume, where the laser-assisted nuclear reactions takes place, and the time interval when the collision events are recorded [31]. Thus, the estimation of the weighting function, that could be the subject of another study, is important in optimizing the experimental conditions. On the other hand, in the realm of high intensity experiments it is known that the limits of focusability and therefore the attainable intensity are dependent on the quality of the beam profile. Therefore we shall contain ourselves to recommend as experimental feature only the condition to ensure a laser intensity of at most $10^{17}\,\mathrm{W/cm^2}$ in the interaction volume. We could

consider either a circular or an eliptical shape of the beam in the interaction area, we could play with a "in-focus" or "out of focus" positioning, but the geometry of an experiment of this kind should also imply data about the heavy ion sources. Therefore we shall not insist here on proposing experimental conditions for a highly efficient interaction. Instead we could comment on the possibility to identify a facility in order to validate some of the predictions made in the present work. A possible laser-assisted heavy-ion scattering (LAHIS) experiment could be sheltered at the NESR storage ring in the framework of the FAIR project (GSI-Darmstadt). This facility is dedicated to light-ion induced reactions in inverse kinematics [32]. In this type of experiment, a beam of light-ions emerging from the storage ring can be scattered on a high-density gas jet of α's, or other light nuclei, and next the reaction products are recorded by a detector in the forward direction. The laser beam could access the volume where nuclear collisions take place, via an aperture operated on the recoil detector and could be supplied by a tabletop laser. A favorable feature is that the gaseous targets have small dimensions and by adjusting the laser pulse duration one optimizes the matter-radiation interaction.

Before ending we mention that it would be also meaningful to extend the present analysis to an arbitrary polarization and to establish how the elliptic polarization of the highly collimated light pulse perturbs the collision in comparison to the linear polarization. Such experimental endeavors are currently carried out [33,34] and are nicely confirming the robustness of the K-W approach.

The authors are indebted to Mrs. C. Matei for carefully reading the manuscript and proposing suggestions in order to improve the text. To Dr. M. Apostol and Dr. M. Ganciu we are grateful for many illuminating discussions. This work was supported by the Institute of Atomic Physics-IFA, through the national programme PN III 5/5.1/ELI-RO, Project 04-ELI/2016 ("QLASNUC") and the Ministry of Research and Innovation of Romania, through the Project PN (ELI) 16 42 01 05/2016.

Author contribution statement

ŞM developed the theoretical formalism, performed the analytic calculations and numerical simulations. FC contributed to the numerical simulations presented in sect. 3.1. ŞM wrote the manuscript and received input from FC for sect. 3.1.

References

1. N.M. Kroll, K.M. Watson, Phys. Rev. A **8**, 804 (1973).
2. F.V. Bunkin, A.E. Kazakov, M.V. Fedorov, Usp. Fiz. Nauk **107**, 559 (1972) Sov. Phys. Usp. **15**, 416 (1973).
3. A. Weingartshofer, C. Jung, *Multiphoton Free-Free Transitions*, in *Multiphoton Ionization of Atoms*, edited by S.L. Chin, P. Lambropoulos (Academic Press, Toronto, 1984) p. 155.
4. D.F. Zaretskii, V.V. Lomonosov, Sov. Phys. JETP **45**, 445 (1977).
5. R.M. Galvão, N.S. Almeida, L.C.M. Miranda, Lett. Nuovo Cimento **38**, 375 (1983).
6. I.F. Barna, S. Varró, Laser Part. Beams **33**, 299 (2015).
7. I.F. Barna, S. Varró, Nucl. Instrum. Methods Phys. B **369**, 77 (2016).
8. Ş. Mişicu, M. Rizea, J. Phys. G **40**, 095101 (2013).
9. W.C. Henneberger, Phys. Rev. Lett. **21**, 838 (1968).
10. K. Alder, A. Winther, *Electromagnetic Excitation-Theory of Coulomb Excitation With Heavy Ions* (North-Holland, Amsterdam, 1975).
11. M. Abramovitz, I. Stegun, *Handbook of Mathematical Functions* (National Bureau of Standards, Washington, 1962).
12. A. Messiah, *Mécanique Quantique*, Tome II (Dounod, Paris, 1960).
13. D.A. Goldberg, S.M. Smith, H.G. Pugh, P.G. Roos, N.S. Wall, Phys. Rev. C **7**, 1938 (1973).
14. G. Hauser *et al.*, Nucl. Phys. A **128**, 81 (1969).
15. J. Albinski *et al.*, Nucl. Phys. A **445**, 477 (1985).
16. J.P. Jeukenne, A. Lejeune, C. Mahaux, Phys. Rev. C **16**, 80 (1977).
17. D. Gogny, *Hartree-Fock Bogolyubov method with density dependent interactions*, in *Proceedings of the International Conference on Nuclear Physics, Munich 1973*, edited by J. de Boer, H.J. Mang, Vol. **1** (North-Holland, Amsterdam, 1974) p. 48.
18. F. Carstoiu, M. Lassaut, Nucl. Phys. A **597**, 269 (1996).
19. J.W. Negele, K. Yazaki, Phys. Rev. Lett. **47**, 71 (1981).
20. M. Beiner, R.J. Lombard, Ann. Phys. (N.Y.) **86**, 262 (1974).
21. I. Angeli, Heavy Ion Phys. **8**, 23 (1998).
22. Ş. Mişicu, F. Carstoiu, Phys. Rev. C **83**, 054622 (2011).
23. Ş. Mişicu, F. Carstoiu, Phys. Rev. C **84**, 051601(R) (2011).
24. D.M. Brink, N. Takigawa, Nucl. Phys. A **279**, 159 (1977).
25. P. Mulser, D. Bauer, *High Power Laser-Matter Interaction*, *Springer Tracts in Modern Physics*, Vol. **228** (Springer, Heidelberg, 2010).
26. F. Negoiţa *et al.*, Rom. Rep. Phys. **68**, S137 (2016).
27. C.J. Joachain, N.J. Kylstra, R.M. Potvliege, *Atoms in Intense Laser Fields* (Cambridge University Press, Cambridge, 2012).
28. J.-C. Diels, W. Rudolph, *Ultrashort Laser Pulse Phenomena*, 2nd edition (Elsevier, Amsterdam, 2006).
29. H. Krüger, Ch. Jung, Phys. Rev. A **17**, 1706 (1978).
30. R. Daniele, G. Ferrante, S. Bivona, J. Phys. B **14**, L213 (1981).
31. A. Weingartshofer, J.K. Holmes, J. Sabbaghit, S.L. Chin, J. Phys. B **16**, 1805 (1983).
32. Yu.A. Litvinov *et al.*, Nucl. Instrum. Methods Phys. B **317**, 603 (2013).
33. M.O. Musa, A. Mac Donald, L. Tidswell, J. Holmes, B. Wallbank, J. Phys. B **43**, 175201 (2010).
34. B.A. de Harak *et al.*, Plasma Sources Sci. Technol. **25**, 035201 (2016).